Contents lists available at ScienceDirect

Atherosclerosis

Translocator protein imaging with ^{18}F-FEDAC-positron emission tomography in rabbit atherosclerosis and its presence in human coronary vulnerable plaques

Kazunari Maekawa [a], Atsushi B. Tsuji [b], Atsushi Yamashita [a,*], Aya Sugyo [b], Chietsugu Katoh [c], Minghui Tang [c], Kensaku Nishihira [d], Yoshisato Shibata [d], Chihiro Koshimoto [e], Ming-Rong Zhang [f], Ryuichi Nishii [b], Keiichiro Yoshinaga [b,1], Yujiro Asada [a]

[a] Department of Pathology, Faculty of Medicine, University of Miyazaki, 889-1692, 5200, Kihara, Kiyotake, Miyazaki City, Miyazaki, Japan
[b] Diagnostic and Therapeutic Nuclear Medicine, National Institute of Radiological Sciences, National Institutes for Quantum and Radiological Science and Technology, 263-8555, 4-9, Anagawa, Inage, Chiba City, Chiba, Japan
[c] Department of Biomedical Science and Engineering, Faculty of Health Sciences, Hokkaido University, 060-0812, 5, 12Jo-Nishi, Kita, Kita-Ku, Sapporo City, Hokkaido, Japan
[d] Department of Cardiology, Miyazaki Medical Association Hospital, 880-2102, 1173, Arita, Miyazaki City, Miyazaki, Japan
[e] Frontier Science Research Center, University of Miyazaki, 889-1692, 5200, Kihara, Kiyotake, Miyazaki City, Miyazaki, Japan
[f] Department of Radiopharmaceuticals Development, National Institute of Radiological Sciences, National Institutes for Quantum and Radiological Science and Technology, 263-8555, 4-9, Anagawa, Inage, Chiba City, Chiba, Japan

ARTICLE INFO

ABSTRACT

Background and aims: This study aimed to investigate whether *N*-benzyl-*N*-methyl-2-[7,8-dihydro-7-(2-[^{18}F]fluoroethyl)-8-oxo-2-phenyl-9H-purin-9-yl]acetamide (^{18}F-FEDAC), a probe for translocator protein (TSPO), can visualize atherosclerotic lesions in rabbits and whether TSPO is localized in human coronary plaques.
Methods: ^{18}F-FEDAC-PET of a rabbit model of atherosclerosis induced by a 0.5% cholesterol diet and balloon injury of the left carotid artery ($n = 7$) was performed eight weeks after the injury. The autoradiography intensity of ^{18}F-FEDAC in carotid artery tissue sections was measured, and TSPO expression was evaluated immunohistochemically. TSPO expression was examined in human coronary arteries obtained from autopsy cases ($n = 16$), and in human coronary plaques ($n = 12$) aspirated from patients with acute myocardial infarction (AMI).
Results: ^{18}F-FEDAC-PET visualized the atherosclerotic lesions in rabbits as high-uptake areas, and the standard uptake value was higher in injured arteries (0.574 ± 0.24) than in uninjured arteries (0.277 ± 0.13, $p < 0.05$) or myocardium (0.189 ± 0.07, $p < 0.05$). Immunostaining showed more macrophages and more TSPO expression in atherosclerotic lesions than in uninjured arteries. TSPO was localized in macrophages, and arterial autoradiography intensity was positively correlated with macrophage concentration ($r = 0.64$) and TSPO ($r = 0.67$). TSPO expression in human coronary arteries was higher in AMI cases than in non-cardiac death, or in the vulnerable plaques than in early or stable lesions, respectively. TSPO was localized in macrophages in all aspirated coronary plaques with thrombi.
Conclusions: ^{18}F-FEDAC-PET can visualize atherosclerotic lesions, and TSPO-expression may be a marker of high-risk coronary plaques.

1. Introduction

Ischemic heart disease and stroke are the leading causes of death and major reasons for loss of quality of life all over the world [1]. The main underlying pathophysiology of ischemic cardiovascular disease is atherosclerosis, leading to thrombosis. Atherosclerosis is a silently progressive chronic inflammatory condition that may become symptomatic suddenly when disruption of an atherosclerotic plaque triggers

thrombus and embolus formation [2]. Vulnerable plaques are characterized by thrombogenic large necrotized cores that are rich in macrophages and T cells, fibrous caps with reduced thickness, and increased neovascularization [3]. For patients with asymptomatic atherosclerosis, it is generally accepted that plaque instability, rather than stenosis, is the most important factor for risk stratification and assessment of therapeutic effects.

Inflammatory activity within carotid atherosclerotic plaques can be identified by positron emission tomography (PET) imaging using ^{18}F-fluorodeoxyglucose (^{18}F-FDG) [4]. Animal studies have confirmed that ^{18}F-FDG uptake is closely correlated with plaque macrophage content and thrombogenic activity [5,6]. Several clinical studies have used ^{18}F-FDG-PET to image coronary plaques [7,8]. However, ^{18}F-FDG uptake by coronary plaques can be obscured by myocardial uptake [9]. Thus, there is a need for novel probes that can highlight macrophage-rich coronary plaques without high accumulation in the myocardium.

Translocator protein (TSPO) is an 18-kDa protein expressed on the outer mitochondrial membrane that displays high binding affinity for cholesterol and drugs. TSPO is upregulated in macrophages, although its function is unclear [10,11], and a number of TSPO-targeted PET tracers have been developed [12–16]. However, the *in vivo* use of these probes for plaque imaging has been unsatisfactory because of a weak target-to-background ratio and/or prominent retention in the walls of vessels without plaque.

We previously developed a TSPO-targeted PET tracer, *N*-benzyl-*N*-methyl-2-[7,8-dihydro-7-(2-[18F]fluoroethyl)-8-oxo-2-phenyl-9H-purin-9-yl]acetamide (^{18}F-FEDAC). In a rat model of pulmonary inflammation, ^{18}F-FEDAC showed high uptake at the inflammation site and low uptake in the heart and blood [17]. In a mouse model of nonalcoholic steatohepatitis, increased liver uptake of ^{18}F-FEDAC was correlated with an increased amount of macrophages and closely linked to disease progression [18]. ^{18}F-FEDAC can also be used for *in vivo* PET imaging of macrophage-induced joint inflammation in mice [19]. Therefore, we hypothesized that ^{18}F-FEDAC could be used to visualize macrophage-rich atherosclerotic plaques in a rabbit model.

Most cases of acute myocardial infarction (AMI) are triggered by coronary plaque disruption and subsequent thrombus formation [20]. Although some studies have shown that TSPO is expressed in human carotid plaques [12,13], no study has examined the expression of TSPO in human coronary plaques. Thus, it remains unknown whether TSPO is expressed in disrupted coronary plaques of AMI patients.

This study aimed to investigate whether ^{18}F-FEDAC-PET can visualize carotid plaques in a rabbit model of atherosclerosis, and whether TSPO is expressed in the human coronary plaques of autopsy cases and AMI patients.

2. Materials and methods

2.1. Compliance with ethical standards

All experimental protocols involving animals were approved by the Animal Care and Use Committee of Miyazaki University (No. 2016–506) and the National Institutes for Quantum and Radiological Science and Technology (No. 16-A036). All animal experiments were conducted in accordance with the institutional guidelines regarding animal care and handling. The histological analysis of human coronary arteries from autopsy cases and coronary thrombi aspirated from AMI patients was approved by the Ethics Committees of the University of Miyazaki, Faculty of Medicine (No. 2015–186 (O) and No. O-0224).

2.2. Rabbit model of carotid atherosclerosis

Seven male Japanese white rabbits, each weighing approximately 2.6–3.0 kg, purchased from Japan SLC (Shizuoka, Japan), were fed a 0.5% cholesterol diet for 1 week prior to transcatheter balloon injury of the right carotid artery. General anesthesia with analgesia was obtained by subcutaneous injection of three-drug mixture including midazolam (2.0 mg/kg), medetomidine (0.5 mg/kg) and butorphanol (0.5 mg/kg), 20 min before the catheter operation. To generate an atherosclerotic lesion, a coronary angioplasty balloon catheter (3.5 mm in diameter; Boston Scientific, MA, USA) was fluoroscopically inserted from the right femoral artery into the right carotid artery, using a guidewire and 4 Fr catheter introducer sheath (Goodman, Nagoya, Japan). Then, the balloon was inflated to 1.5 atm and the carotid artery was denuded of endothelial cells with the inflated balloon. The procedure was performed according to a previously reported model with modifications of the insert-site of the balloon catheter and the injured artery [6]. Eight weeks after the balloon injury, rabbits underwent the imaging procedure.

2.3. ^{18}F-FEDAC positron emission tomography and computed tomography

Seven rabbits (body weight 3.33 ± 0.17 kg) were injected with ^{18}F-FEDAC (251 ± 27 MBq) via the auricular vein 3 h before PET imaging. The rabbits were placed under isoflurane anesthesia (1.5–2.0%), and PET was conducted for 30 min using an Inveon small-animal PET system (Siemens Medical Solutions, Malvern, PA, USA), followed by contrast-enhanced computed tomography (CE-CT) (CosmoScan GXII, Rigaku, Tokyo, Japan). PET images were reconstructed using a 3D maximum a posteriori algorithm (18 iterations with 16 subsets) without attenuation correction. The region of interest was manually drawn over the blood vessels, and tracer uptake was quantified in terms of standardized uptake value (SUV) using the reconstructed PET images. For CE-CT, a contrast agent was injected intravenously (3 mL/kg iopamidol with 370 mg/mL iodine; Oiparomin 370, Fuji Pharmaceutical Co., Toyama, Japan), and blood vessels were imaged 20 s after injection. CT images were acquired with an X-ray source set at 90 kVp and 200 μA using a small-animal CT system (CosmoScan GXII, Rigaku, Tokyo, Japan) and were reconstructed using a filtered back-projection algorithm for cone beam.

2.4. Radioactivity of blood and tissues

Immediately after PET and CE-CT imaging, rabbits were euthanized by pentobarbital sodium injection to permit measurement of the biodistribution of the radioactive tracer. The blood, bilateral carotid arteries, left ventricular myocardium, lungs, liver, kidneys, pancreas, and skeletal muscle were excised and weighed. Blood and tissue radioactivity were measured using a gamma counter (2480 Wizard2; PerkinElmer, Waltham, MA, USA). Data were recorded in terms of the SUV.

2.5. Autoradiography

After the biodistribution study, the excised myocardium and the carotid arteries (right and left) were embedded in Tissue-Tek optimal cutting temperature compound (Sakura Finetek Japan, Tokyo, Japan). Frozen microsections (20 μm thick) were placed on glass slides, dried, and exposed to an imaging plate (GE Healthcare, Chicago, IL, USA). The imaging plate was read using an FLA-7000 imaging plate reader (GE Healthcare). The radiographic intensities of the myocardium and arteries were measured using ImageJ software (National Institutes of Health, Bethesda, MD, USA). 28 sections of the uninjured artery and 32 sections of the injured artery were processed, and the ratio of arterial intensity to myocardial intensity was recorded for both uninjured and injured arteries.

2.6. Histology and immunohistochemistry of the rabbit carotid artery

Autoradiography (ARG), HE stained section, and sections for the immunohistochemical study were serial sections of the same lesions (same tissue blocks). Serial tissue microsections corresponding to those

examined by autoradiography were stained with hematoxylin and eosin (Sakura Finetek Japan) or labeled with primary antibodies against TSPO (goat polyclonal, ORIGENE, Rockville, MD, USA), rabbit macrophages (RAM11, mouse monoclonal, DAKO, Santa Clara, CA, USA), and smooth muscle actin (SMA) (1A4, mouse monoclonal, DAKO). Peroxidase-labeled secondary antibodies (EnVision system, DAKO) were used to stain areas labeled with primary antibodies. Localization of proteins was visualized with 3,3'-diaminobenzidine. Histological and immunohistochemical slides were scanned using a NanoZoomer slide scanner (Hamamatsu Photonics, Hamamatsu, Japan) for imaging analysis. Areas where immunostaining was positive for TSPO, macrophages, and SMA were assessed using a color imaging morphometry system (WinROOF, Mitani, Tokyo, Japan).

2.7. TSPO expression in human coronary arteries in autopsy cases

Human coronary arteries were obtained from autopsy cases performed at University of Miyazaki Hospital, including 6 cases who died of non-cardiac causes (control group), 5 cases who died of non-cardiac disease but with old myocardial infarction (OMI, OMI group), and 5 cases who died of AMI (AMI group). Coronary arteries were formalin-fixed, paraffin-embedded, and thin-sliced into 3 μm-thick for histological analysis. Seven to 11 arterial sections from the proximal portion of right and left coronary arteries were obtained from each case. The AMI group included culprit lesions. Coronary plaques were classified into early lesion (diffuse intimal thickening), stable lesion (pathological intimal thickening, fibroatheroma or fibroatheroma with macrocalcification), or vulnerable lesion (thin cap fibroatheroma, intraplaque hemorrhage or ruptured plaque) (Supplementary Table 1), according to Virmani et al. [21]. Then, coronary arteries were immunohistochemically analyzed using primary antibodies against TSPO (ab109497, rabbit monoclonal, Abcam, Cambridge, UK), CD68 (DAKO) and smooth muscle actin (1A4, mouse monoclonal, DAKO) visualized with the EnVision system (DAKO). Percentage of the areas positively stained for these antibodies in coronary arteries was assessed using a color imaging morphometry system (WinROOF).

2.8. Expression of TSPO in disrupted human coronary plaques with thrombi in patients with AMI

Human coronary plaques with thrombi were obtained through coronary thrombus aspiration during percutaneous coronary intervention for AMI at the Department of Cardiology, Miyazaki Medical Association Hospital, Japan. From 234 consecutively treated patients, we selected the aspirated thrombi with the largest plaque components ($n = 12$, plaque area >1.5 mm^2). Thrombus samples were formalin-fixed, paraffin-embedded, and thin-sliced to 3 μm for histological analysis. Immunohistochemistry was performed using primary antibodies against TSPO (Abcam) and CD68 (DAKO), detected with the EnVision system (DAKO). Areas in coronary plaques where immunostaining was positive for TSPO and macrophages were assessed using a color imaging morphometry system (WinROOF).

2.9. Statistics

All statistical calculations were conducted using GraphPad Prism software (version 8.0.1; GraphPad Software, San Diego, CA, USA). Data are shown as the mean ± standard deviation. Comparisons between two groups were performed using the Wilcoxon signed-rank test. Comparisons among three groups were performed using the Kruskal–Wallis test followed by Dunn's multiple comparison test. Spearman's rank correlation coefficient was used for the correlation analysis. Statistical significance was set at $p < 0.05$.

3. Results

3.1. ^{18}F-FEDAC PET and contrast-enhanced CT in a rabbit atherosclerosis model

Representative axial and sagittal images of the rabbit model, taken with ^{18}F-FEDAC-PET and CE-CT, are shown in Fig. 1A and B. ^{18}F-FEDAC-PET showed higher ^{18}F-FEDAC uptake along the right side of the trachea, corresponding to the injured right carotid artery, than along the left side of the trachea, corresponding to the uninjured left carotid artery (Fig. 1A). The luminal diameters of the injured right carotid arteries showed subtle or insignificant changes on contrast-enhanced CT in comparison with uninjured left carotid arteries (Fig. 1B). The mean SUV of the injured right carotid arteries (0.28 ± 0.06) was significantly higher than that of the uninjured left carotid arteries (0.20 ± 0.05; $n = 7$ for each, $p < 0.05$). The maximum SUV of the injured right carotid arteries (0.31 ± 0.08) was also significantly higher than that of the uninjured left carotid arteries (0.24 ± 0.07; $n = 7$ for each, $p < 0.05$) (Fig. 1C).

3.2. Biodistribution of ^{18}F-FEDAC in extracted tissues

Supplementary figure 1 shows a representative macrophotograph of the carotid arteries just before their excision after PET and CE-CT imaging. Injured right carotid arteries were yellowish-white in color and enlarged compared with uninjured left carotid arteries. Neovascularization was observed in the adventitia of the right carotid arteries. These findings were compatible with the development of atherosclerotic lesions in the right carotid arteries.

Among the tissues extracted, SUVs for ^{18}F-FEDAC uptake were highest in the injured carotid artery (0.57 ± 0.24), lungs (0.54 ± 0.21), liver (0.63 ± 0.20), and kidneys (0.65 ± 0.22) ($n = 7$ for each). The mean SUV of the injured right carotid arteries (0.57 ± 0.24) was significantly higher than that of the uninjured left carotid arteries (0.28 ± 0.13; $n = 7$, $p < 0.05$) or the myocardium (0.19 ± 0.07, $n = 7$, $p < 0.05$) (Fig. 2A). The mean artery-to-blood intensity ratio was significantly higher in the injured arteries (1.62 ± 0.53) than in the uninjured arteries (0.76 ± 0.25; $n = 7$, $p < 0.05$). Likewise, the mean artery-to-myocardium intensity ratio was significantly higher in the injured arteries (3.10 ± 0.93) than in the uninjured arteries (1.45 ± 0.45; $n = 7$, $p < 0.05$) (Fig. 2B).

3.3. Autoradiography and histological examination

Artery-to-myocardium intensity ratio, as measured with autoradiographic imaging of ^{18}F-FEDAC, was higher in the arterial wall of the injured arteries (2.24 ± 0.86, $n = 32$) than that in the arterial wall of the uninjured arteries (0.97 ± 0.51, $n = 28$; $p < 0.0001$) (Fig. 3A). Fig. 3B shows representative autoradiographic and histological images of the uninjured and injured arteries. Compared to uninjured arteries, injured arteries showed higher radio signal intensity in ARG, thicker arterial wall with neointimal formation, infiltration of macrophages, smooth muscle cell (SMC) proliferation, and extracellular matrix deposition. Focal SMC disappearance in the medial layer was also noted. TSPO was predominantly localized in macrophages in the atherosclerotic neointima, but sparsely in the media, and a slight degree of TSPO expression was observed in some of the uninjured arteries (Fig. 3B and C). The arterial wall area was significantly larger in injured arteries (1.91 ± 0.87 mm^2, $n = 32$) than in the uninjured arteries (0.68 ± 0.18 mm^2, $n = 28$; $p < 0.0001$). Areas immunopositive for macrophages and TSPO were significantly larger in injured arteries (macrophage area 21.7 ± 13.3%, TSPO area 5.4 ± 4.6%, $n = 32$) than in uninjured arteries (macrophage area 1.4 ± 1.5%, TSPO area 0.6 ± 1.0%, $n = 24$; $p < 0.0001$ in each). The area immunopositive for SMA was smaller in injured arteries (34.5. ± 12.1%, $n = 32$) than uninjured arteries (49.5 ± 10.6%, n = 24, $p < 0.0001$) (Fig. 3 D).
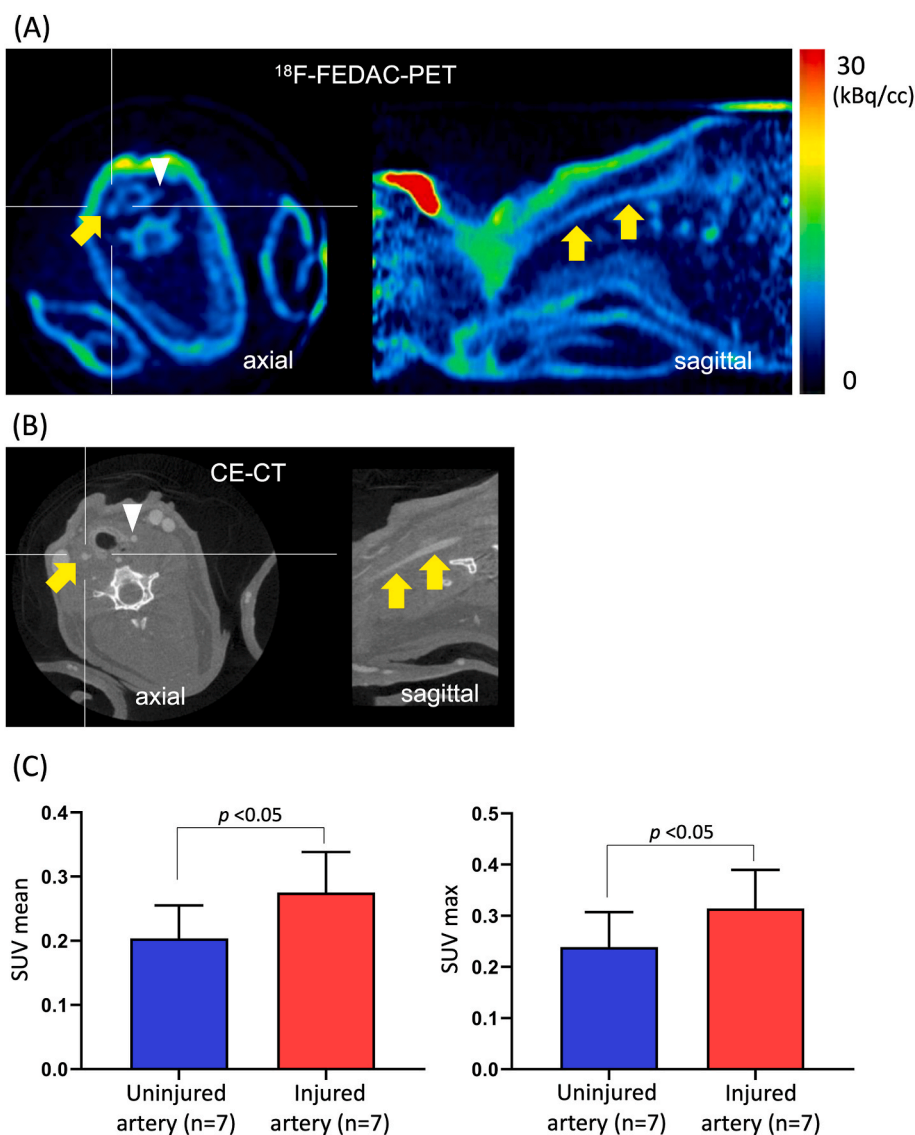
Fig. 1. ^{18}F-FEDAC-positron emission tomography and contrast-enhanced computed tomography of a rabbit atherosclerosis model.
(A) Representative axial and sagittal images of ^{18}F-FEDAC-positron emission tomography. The axial image shows higher ^{18}F-FEDAC uptake along the right side of the trachea (arrow) corresponding to the injured right carotid artery, compared to the left side of the trachea (arrowhead) corresponding to the un-injured left carotid artery. The sagittal image matching a white vertical line in the axial image shows high ^{18}F-FEDAC uptake which corresponds to the right carotid artery (arrows). (B) Representative axial and sagittal images of contrast enhanced computed to-mography. The contrast enhanced uninjured left (arrowhead) and injured right (arrow) carotid arteries show no significant difference in the luminal size on the axial image. The sagittal image corresponding to white vertical line in the axial image shows the right carotid artery (arrows). (C) Standardized uptake value on body weight (SUVbw) of uninjured left and injured right carotid arteries. n = 7 in each, Wilcoxon signed rank test.

The artery-to-myocardium intensity ratio was positively correlated with the areas immunopositive for macrophages (RAM11) ($r = 0.64$, $n = 56$, $p < 0.001$) and TSPO ($r = 0.67$, $n = 56$, $p < 0.0001$), but negatively correlated with the areas immunopositive for SMA ($r = -0.67$, $n = 56$, $p < 0.0001$) (Fig. 3E).

3.4. TSPO expression in human coronary arteries in autopsy cases

To determine TSPO expression in human coronary artery, we histo-logically analyzed the proximal portion of right and left coronary ar-teries from autopsy cases of non-cardiac death without OMI (control group, n = 6, 49 coronary sections), non-cardiac death with OMI (OMI group, n = 5, 39 coronary sections), and cardiac death due to AMI (AMI group, n = 5, 38 coronary sections including culprit lesions). Clinical background of autopsy cases is shown in Supplementary Table 2. Among these 126 coronary artery sections, 27 were classified as early lesions, 77 were stable lesions and 22 were vulnerable lesions. Coronary plaques of the control group consisted of 27 early lesions and 22 stable lesions but no vulnerable lesions. Coronary plaques of the OMI group consisted of no early lesion, 35 stable lesions, and 4 vulnerable lesions. Coronary plaques of the AMI group consisted of no early lesion, 20 stable lesions, and 18 vulnerable lesions (Supplementary Fig. 2). Immunohistochemi-cally, CD68$^-$ and TSPO-positive cells were predominantly localized in

atherosclerotic plaques. In the atherosclerotic plaque, TSPO expressing cells were predominantly CD68-positive macrophages. In addition, a part of SMA-positive SMCs expressed TSPO in the vulnerable plaques (Fig. 4A and B). CD68 and TSPO positive areas in the coronary arteries of the AMI group were significantly larger than those of the control ($p < 0.0001$) or the OMI groups ($p < 0.01$). Likewise, in comparison to plaque types, CD68 and TSPO positive areas in coronary arteries with vulner-able lesions were significantly larger than those with early ($p < 0.0001$) or stable lesions ($p < 0.0001$). SMA-positive areas in the coronary ar-teries of the AMI group were significantly smaller than those of the control ($p < 0.0001$) or the OMI groups ($p < 0.05$), and SMA-positive areas in the coronary arteries with vulnerable lesions were signifi-cantly smaller than those with early or stable lesions (both $p < 0.0001$) (Fig. 4C and D).

3.5. TSPO expressing macrophages in coronary thrombi in patients with AMI

To determine whether TSPO-expressing cells were present in coro-nary culprit plaques with thrombi, we examined coronary aspiration tissue samples from 12 AMI patients, which contained fresh thrombi and ruptured plaque components. Clinical characteristics of patients are shown in Supplementary Table 3. The average age of the patients was
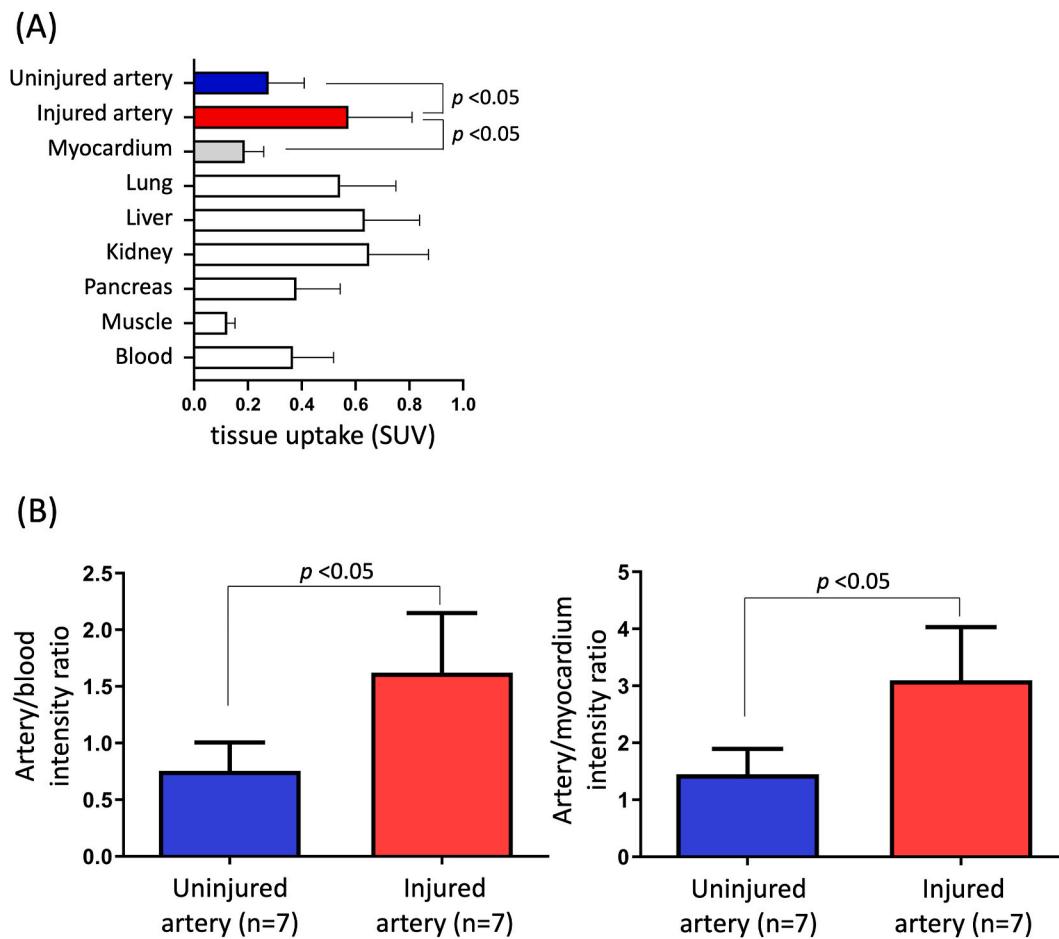
(A)

(B)

Fig. 2. Tissue distribution and artery-to-blood or artery-to-myocardium radioactivity ratios of ^{18}F-FEDAC.
(A) Weight adjusted standardized uptake values in tissues show higher ^{18}F-FEDAC uptake in the injured right carotid artery, lung, liver, and kidney. n = 7 in each, Wilcoxon signed rank test. (B) Artery-to-blood or artery-to-myocardium radioactivity ratio. n = 7 in each, Wilcoxon signed rank test.

63.2 (range 42–88) years; 10 patients were male (83%) and 8 were smokers (67%). One-third of the patients developed AMI while receiving antiplatelet therapy. The coronary thrombi were aspirated from the right coronary artery (n = 6) or left anterior descending artery (n = 6). In all 12 cases, a positive immunoreaction for TSPO was observed in macrophages in the disrupted plaques, causing thrombus formation (Fig. 5). The areas immunopositive for TSPO and CD68 in the disrupted plaques were $6.0 \pm 5.6\%$ and $10.7 \pm 8.2\%$, respectively (Supplementary Table 4).

4. Discussion

In the present study, we successfully tested PET imaging of TSPO with ^{18}F-FEDAC in a rabbit atherosclerosis model and found enhanced TSPO expression in human coronary arteries in AMI cases and vulnerable plaques, and the presence of TSPO-expressing macrophages in coronary culprit lesions in AMI patients. ^{18}F-FEDAC-PET may be a useful imaging tool for detecting rupture-prone macrophage-rich plaques in the coronary artery.

Several previous studies have focused on PET imaging targeting TSPO in atherosclerotic mouse models, with atherosclerosis being induced by cuff-induced injury or apolipoprotein E knockout; however, the results of these studies were inconsistent. Some of them reported high tracer uptake in lesions, but others did not [22–24]. These discrepancies may be due to the low spatial resolution of PET in mouse models (1–2 mm). In this study, we employed a rabbit model of carotid artery atherosclerosis. We considered this model more suitable for PET

studies because the rabbit carotid artery is 2–3 times larger in diameter than the mouse aorta and because, for anatomical reasons, the injured and uninjured carotid arteries could easily be compared in the axial view. Gaemperli et al. examined human carotid atherosclerosis using PET/CT angiography with the TSPO ligand ^{11}C-PK11935 in patients with symptomatic (stroke or transient ischemic attack) and asymptomatic carotid stenosis. ^{11}C-PK11935 uptake was higher in symptomatic carotid plaques than in asymptomatic plaques; however, the target-to-background ratio was too low (1.06/0.20) to highlight the lesions [13]. This might be due to slow washout of the tracer from the lesions. The half-life of ^{11}C is 20 min, which is not appropriate for delayed imaging, while that of ^{18}F is 110 min, enabling delayed imaging. Our preliminary study showed higher contrast in images taken 3 h after injection than in images taken 2 h after injection (data not shown). Uptake of ^{18}F-FEDAC 3 h after injection was 1.6 times higher in injured carotid artery tissue than in blood (Fig. 2B). Thus, the time between ^{18}F-FEDAC injection and PET imaging may affect the results *in vivo*.

^{18}F-FEDAC accumulation as determined by autoradiography was approximately two times higher in injured carotid arteries than in uninjured arteries (Fig. 3A). These results were comparable with those observed for *in vivo* ^{18}F-FEDAC-PET imaging. However, previous clinical and preclinical studies reported no significant difference in radioactivity between the uninjured and atherosclerotic arteries. No significant difference was found between symptomatic and asymptomatic patients with regard to plaque uptake of the TSPO tracers ^{3}H-PK11195 (as measured by autoradiography) or ^{11}C-PK11195 (in terms of SUV) [13]. In previous animal studies, autoradiographic analysis of the
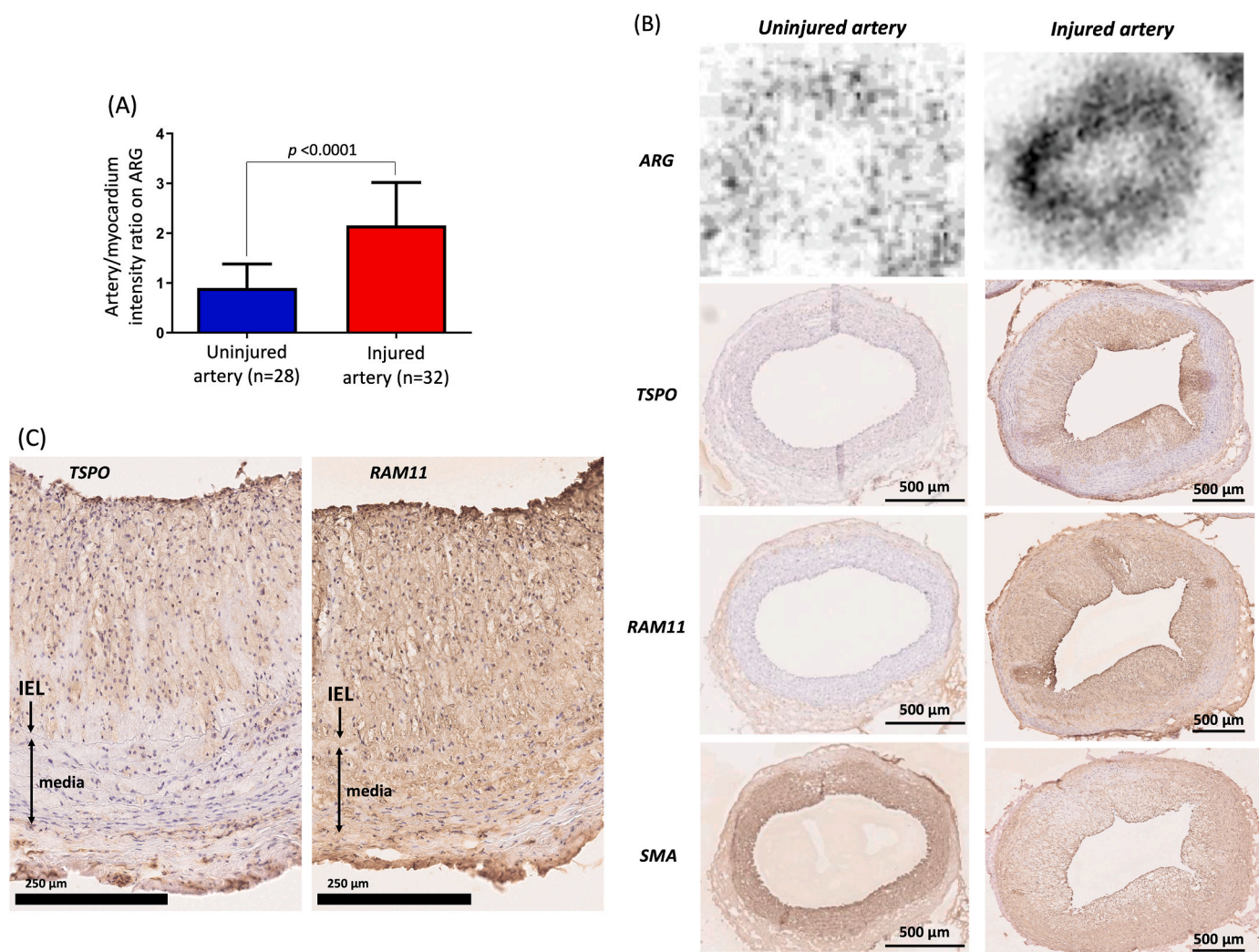
Fig. 3. ^{18}F-FEDAC autoradiography and TSPO expression in rabbit carotid arteries.
(A) Artery-to-myocardium intensity ratio on ^{18}F-FEDAC autoradiography (ARG) between uninjured and injured carotid arteries. Mann-Whitney u-test. (B) Representative images of ARG and corresponding immunohistochemical images for translocator protein (TSPO), rabbit macrophages (RAM11) and smooth muscle actin (SMA) of uninjured left and injured right carotid arteries. Compared to the uninjured artery, the injured artery shows higher uptake signal of ^{18}F-FEDAC on ARG and thicker neointimal formation, which shows infiltrate of dense macrophages and lessor smooth muscle cells. TSPO expression is predominantly localized in the neointima. Scale bars represent 500 μm. (C) High magnification images of immunohistochemistry for TSPO and RAM11 in the injured carotid artery. TSPO expression is predominantly localized in macrophage-positive area in the atherosclerotic neointima. IEL, internal elastic lamina. Scale bars represent 250 μm. (D) Wall area and immunopositive areas for RAM11, SMA, and TSPO in uninjured and injured carotid arteries. Mann-Whitney *U* test. (E) Relationship between artery-to-myocardium intensity ratio on ^{18}F-FEDAC autoradiography and immunopositive areas for RAM11, SMA, and TSPO. n = 56 in each, r, Spearman's rank correlation coefficient.

radiolabeled ligands ^{18}F-FEMPA, ^{18}F-GE-180, and ^{11}C-PK11195 did not show any difference in uptake between atherosclerotic and normal aorta [14,15,20]. A study using rat brain homogenate found that although FEDAC had a lower binding affinity for the peripheral benzodiazepine receptor than PK11195, the lipophilicity of PK11195 was higher than that of FEDAC [25]. This suggests that nonspecific binding of PK11195 reduces its specificity for TSPO. In contrast, the positive correlation of ^{18}F-FEDAC signals with macrophages and TSPO densities suggests that the ligand has good binding specificity for TSPO.

The TSPO ligands ^{11}C-PK11195, ^{18}F-GE-180, and ^{18}F-FEDAC each showed different tissue distributions. In both low-density lipoprotein receptor–deficient and apolipoprotein B48–deficient mice, the radiographic intensity of ^{11}C-PK11195 20 min after injection was highest in the lung, heart, and liver; aortic intensity was approximately one-half of that in the heart [24]. In the two same mouse models, the intensity of ^{18}F-GE-180 60 min after injection was highest in the adrenal gland, kidney, and lung; aortic intensity was similar to that in the heart [15]. In

our study of rabbits fed a 0.5% cholesterol diet, the intensity of ^{18}F-FEDAC was highest in the kidney, liver, injured artery, and lung. Interestingly, the intensity ratio of the atherosclerotic artery to the myocardium was approximately 3.0. This high uptake ratio could make PET with ^{18}F-FEDAC highly suitable for clinical application in patients with coronary atherosclerosis.

The present study revealed that TSPO was expressed in both rabbit carotid plaques and human coronary atherosclerotic plaques and culprit plaques associated with coronary thrombi. Our autopsy study suggests that the enhanced TSPO expression in coronary arteries of the AMI group is due to increase of TSPO-expressing macrophages in the vulnerable plaques. TSPO expression in cultured macrophages is downregulated by the proinflammatory stimuli of lipopolysaccharide and interferon-γ but not by the alternative stimuli of interleukin-4, dexamethasone or tumor growth factor-β [11]. Kim et al. conducted transcriptome analysis using single-cell RNA-sequencing of CD45-positive cells obtained from atherosclerotic murine aorta [26].
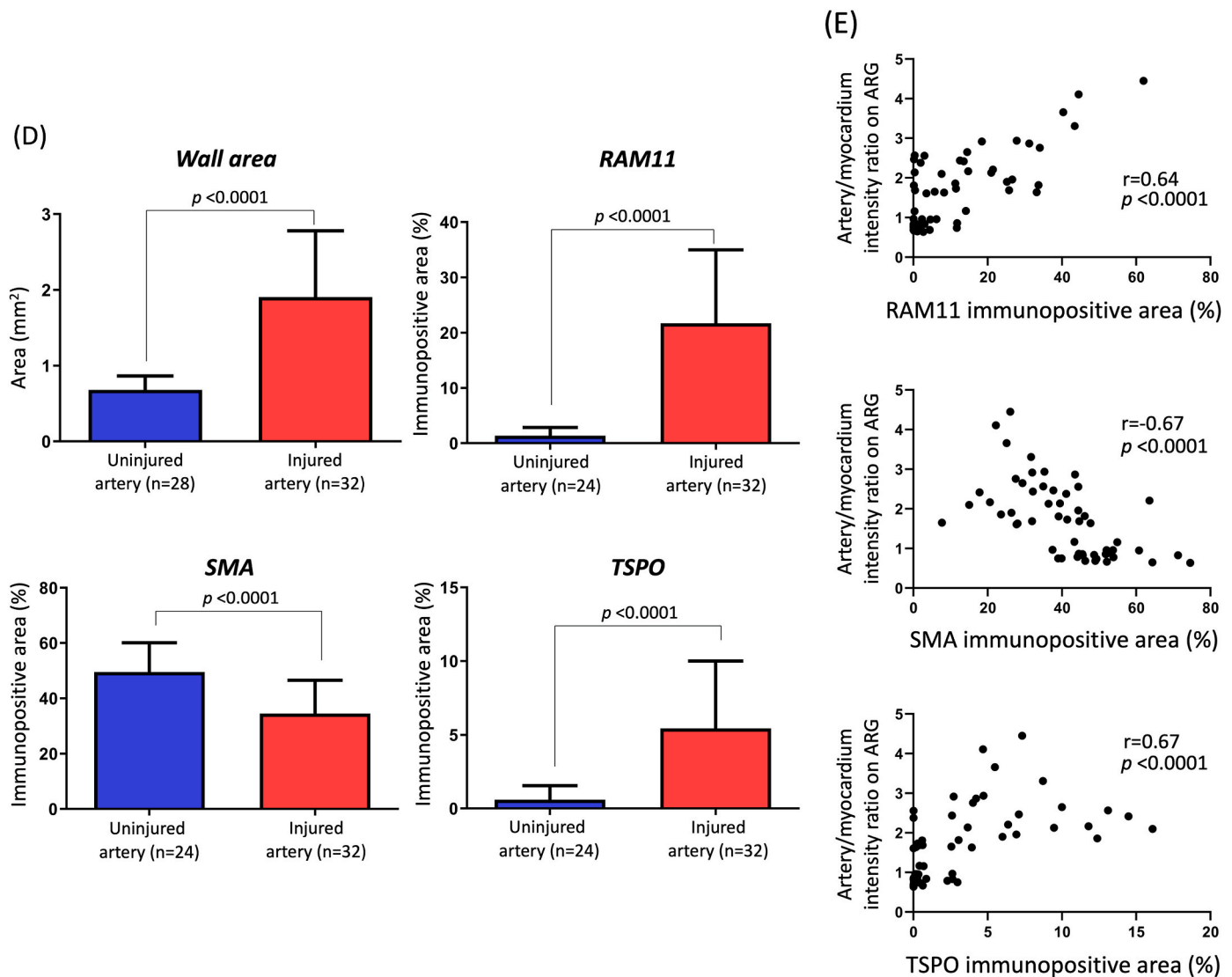
Fig. 3. (*continued*).

They found that TSPO expression was increased in macrophage clusters expressing CD163 and chemokine (C–C motif) ligand 24 as well as in those expressing CD63 and TREM2 (triggering receptor expressed on myeloid cells 2) but was decreased in macrophage clusters expressing CD209a and S100A4 as well as in those expressing lymphocyte activation protein 6a and chemokine (C-X-C motif) ligand 10. Evidence suggests that the plaque microenvironment and macrophage phenotype may affect TSPO expression in atherosclerotic arteries. In fact, in human coronary atherosclerotic plaques, TSPO expression was noted predominantly in macrophages surrounding a necrotic core, but not in all the macrophages. In addition, TSPO-expressing macrophages are present in coronary thrombi in patients with AMI. These findings indicate that the majority of macrophages in coronary culprit plaques express TSPO and that plaque disruption triggers exposure of these macrophages to the coronary circulation and subsequent thrombus formation. Given the contribution of TSPO-expressing macrophages to coronary thrombus formation, noninvasive detection of TSPO in the coronary artery may be of great clinical importance.

^{18}F-FDG-PET is very useful for evaluating inflammatory disease and already in clinical use for carotid plaque imaging [27]; however, it is not suitable for coronary plaque imaging due to high ^{18}F-FDG uptake in the myocardium. In our rabbit model of atherosclerosis, ^{18}F-FEDAC uptake was significantly higher in the atherosclerotic artery than in the myocardium and uninjured artery. We used ^{18}F rather than ^{11}C to radiolabel our ligand because it has significant advantages for clinical PET imaging, as an on-site cyclotron is not required, and imaging can be delayed for a greater lesion-to-background ratio. In addition, we found that the target molecule, TSPO, was expressed in coronary culprit plaques, including in patients undergoing secondary prevention. Our animal and human pathological studies suggest that ^{18}F-FEDAC is a promising probe for coronary atherosclerosis imaging, and its feasibility for this purpose warrants further clinical study.

This study has several limitations. First, we did not perform PET/CT. Therefore, localization of lesions that showed high uptake on PET relied on separate CT images. However, the targeting accuracy of our *in vivo* PET imaging is supported by the longitudinal localization of the high-uptake lesions along the right side of the trachea and the *ex vivo* high radiographic intensity of the atherosclerotic right carotid artery. Second, we did not compare ^{18}F-FEDAC uptake in the carotid arteries and heart *in vivo* because the field of view was too small to cover the entire area from the carotid arteries to the heart. Instead, we performed *ex vivo* tissue distribution analysis and autoradiography of the carotid arteries and myocardium of the left ventricle. Third, the low target to background ratio is a concern with the ^{18}F-FEDAC PET imaging. One of the reasons of this issue may be relatively low vessel to blood ratio. Blood radioactivity may affect the contrast between the atherosclerotic artery
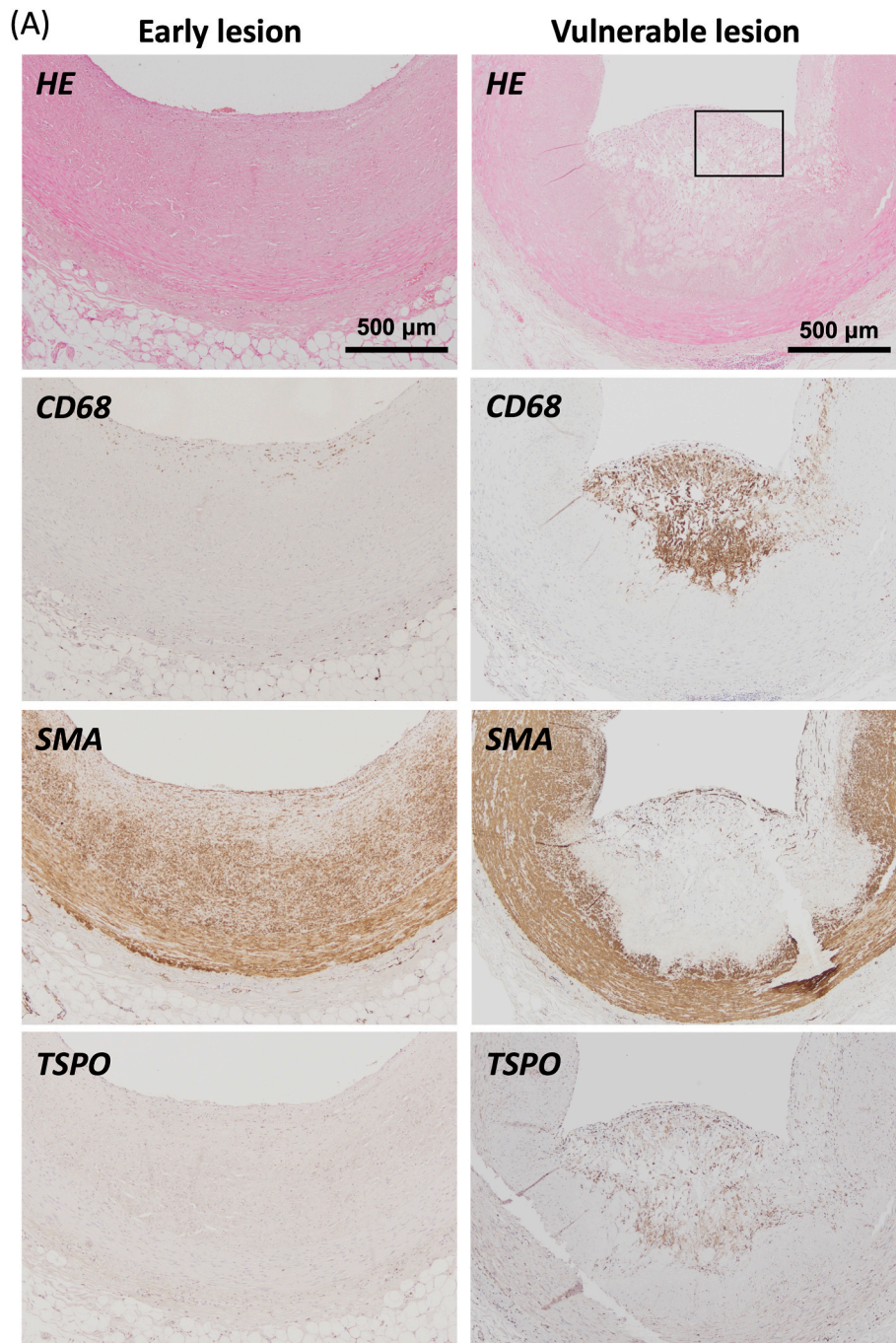
Fig. 4. TSPO expression in coronary arteries from autopsy cases.
(A) Representative microphotographs of early and vulnerable lesions. In the vulnerable lesion, CD68 positive cells are accumulated in and around the necrotic core, associated with broad loss of SMA positive cells. TSPO positive cells are colocalized with part of CD68 positive cells. The early lesion shows only sparce distribution of CD68 positive cells with no evident TSPO positive cells, although SMA positive cells diffusely present. (B) High magnification view of the lined box on Fig. 4A. TSPO expression is mainly observed in macrophages, also weakly seen in smooth muscle cells in a vulnerable plaque. (C) CD68, SMA and TSPO immunopositive areas in coronary arteries from autopsy cases of non-cardiac death without OMI (control), non-cardiac death with OMI (OMI), and cardiac death due to AMI (AMI). Kruskal–Wallis test followed by Dunn's multiple comparison test. (D) CD68, SMA and TSPO immunopositive areas in coronary arteries with early, stable, and vulnerable lesions. Kruskal–Wallis test followed by Dunn's multiple comparison test.
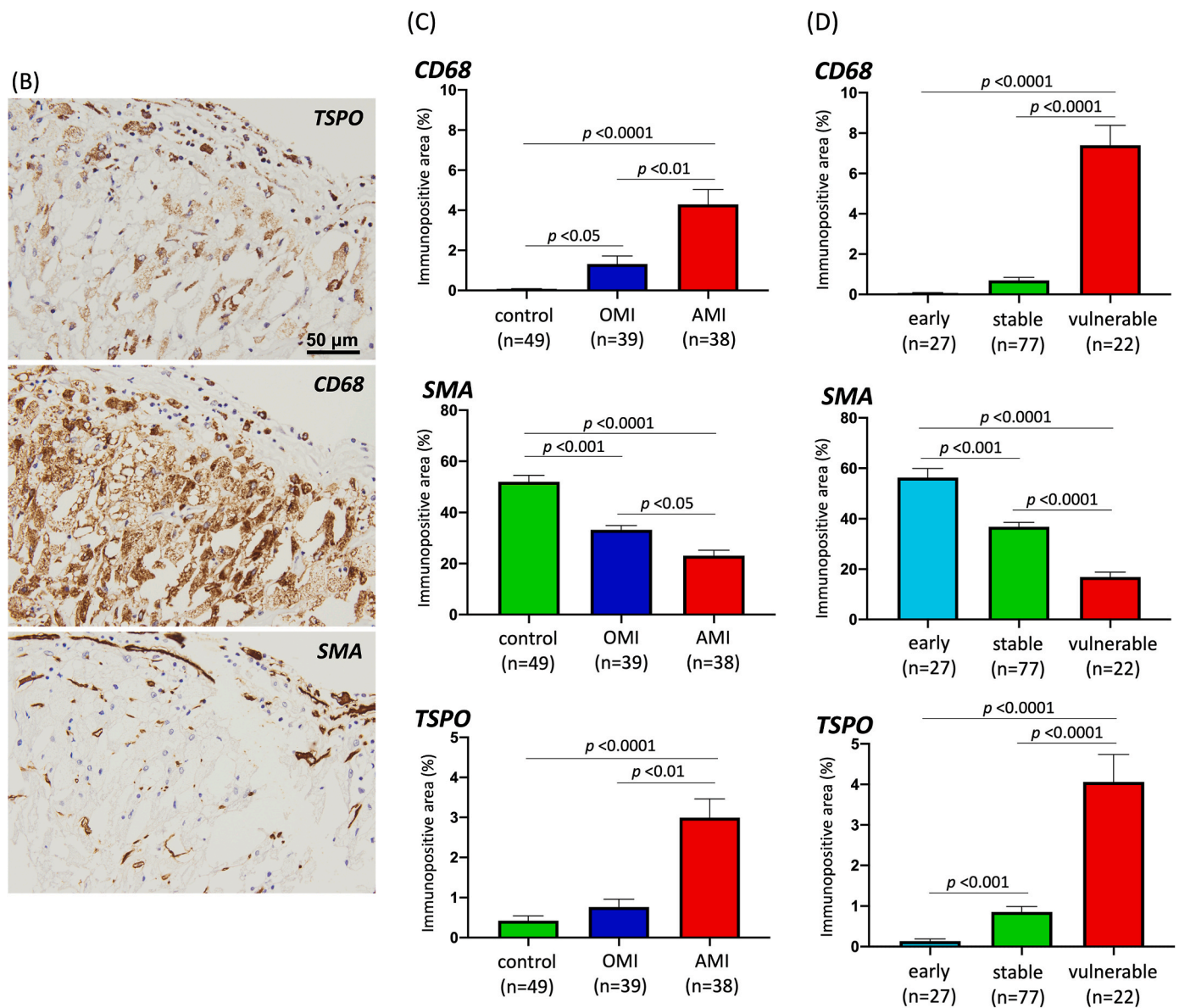
(B)

TSPO

50 µm

CD68

SMA

(C)

CD68

Immunopositive area (%)

$p < 0.0001$
$p < 0.01$
$p < 0.05$

control (n=49)   OMI (n=39)   AMI (n=38)

SMA

Immunopositive area (%)

$p < 0.0001$
$p < 0.001$
$p < 0.05$

control (n=49)   OMI (n=39)   AMI (n=38)

TSPO

Immunopositive area (%)

$p < 0.0001$
$p < 0.01$

control (n=49)   OMI (n=39)   AMI (n=38)

(D)

CD68

Immunopositive area (%)

$p < 0.0001$
$p < 0.0001$

early (n=27)   stable (n=77)   vulnerable (n=22)

SMA

Immunopositive area (%)

$p < 0.0001$
$p < 0.001$
$p < 0.0001$

early (n=27)   stable (n=77)   vulnerable (n=22)

TSPO

Immunopositive area (%)

$p < 0.0001$
$p < 0.0001$
$p < 0.001$

early (n=27)   stable (n=77)   vulnerable (n=22)

Fig. 4. (*continued*).

and the control artery due to close localization of the arteries and the blood *in vivo*. Fourth, the ^{18}F-FEDAC-PET study was based on experimental animal models, which might differ from naturally developed atherosclerosis. In fact, the mean value of macrophage immunopositive area in the human AMI group (4.5%) was smaller than that in rabbit injured arteries (20%). However, the mean values of TSPO immunopositive area in the AMI group (3%) and the vulnerable plaques (4%) were close to those in rabbit injured arteries (5%). Therefore, a clinical study is required to show usefulness of the ^{18}F-FEDAC-PET in patients with atherosclerotic disease.

^{18}F-FEDAC-PET imaging targeting TSPO was able to visualize macrophage-rich atherosclerotic plaques in rabbits. TSPO-expressing macrophages are present in human coronary vulnerable plaques and thrombus associated coronary culprit plaques in patients with AMI. ^{18}F-FEDAC-PET is a potential candidate for non-invasive detection of high-risk coronary plaques.

CRediT authorship contribution statement

Kazunari Maekawa: Methodology, Formal analysis, Investigation, Resources, Writing – original draft, Visualization. **Atsushi B. Tsuji:** Methodology, Formal analysis, Investigation, Writing – original draft, Visualization. **Atsushi Yamashita:** Conceptualization, Methodology, Investigation, Writing – review & editing. **Aya Sugyo:** Formal analysis,
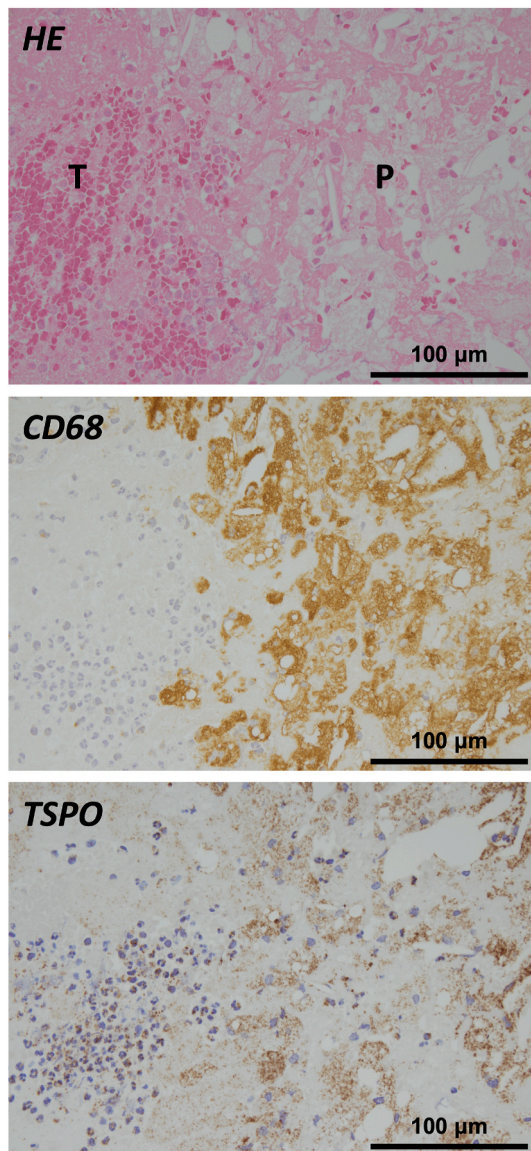
Fig. 5. TSPO expression in coronary atherothrombotic plaque in a patient with acute myocardial infarction.
The histological image of hematoxylin-eosin (HE) stain shows disrupted plaque component (P) with thrombus formation (T). Immunohistochemistry shows the presence of translocator protein (TSPO) positive macrophages (CD68) in the disrupted plaque component and direct contact to the thrombus. Scale bars represent 100 μm.

Investigation, Writing – original draft, Visualization. **Chietsugu Katoh:** Formal analysis. **Minghui Tang:** Formal analysis. **Kensaku Nishihira:** Resources. **Yoshisato Shibata:** Resources. **Chihiro Koshimoto:** Resources. **Ming-Rong Zhang:** Resources. **Ryuichi Nishii:** Conceptualization, Writing – review & editing, Supervision, Project administration. **Keiichiro Yoshinaga:** Conceptualization, Writing – review & editing, Supervision. **Yujiro Asada:** Writing – review & editing, Supervision, Project administration.

Declaration of competing interest

The authors declare that they have no known competing financial interests or personal relationships that could have appeared to influence the work reported in this paper.

Appendix A. Supplementary data

Supplementary data to this article can be found online at https://doi.org/10.1016/j.atherosclerosis.2021.10.003.

References

[1] P. Joseph, D. Leong, M. McKee, S.S. Anand, J.D. Schwalm, K. Teo, A. Mente, S. Yusuf, Reducing the global burden of cardiovascular disease, Part 1: the epidemiology and risk factors, Circ. Res. 121 (2017) 677–694, https://doi.org/10.1161/CIRCRESAHA.117.308903.

[2] G.K. Hansson, P. Libby, I. Tabas, Inflammation and plaque vulnerability, J. Intern. Med. 278 (2015) 483–493, https://doi.org/10.1111/joim.12406.

[3] P.K. Shah, E. Falk, J.J. Badimon, A. Fernandez-Ortiz, A. Mailhac, G. Villareal-Levy, J.T. Fallon, J. Regnstrom, V. Fuster, Human monocyte-derived macrophages induce collagen breakdown in fibrous caps of atherosclerotic plaques. Potential role of matrix-degrading metalloproteinases and implications for plaque rupture, Circulation 92 (1995) 1565–1569.

[4] J.H. Rudd, E.A. Warburton, T.D. Fryer, H.A. Jones, J.C. Clark, N. Antoun, P. Johnström, A.P. Davenport, P.J. Kirkpatrick, Arch BN et al. Imaging atherosclerotic plaque inflammation with [18F]-fluorodeoxyglucose positron emission tomography, Circulation 105 (2002) 2708–2711, https://doi.org/10.1161/01.cir.0000020548.60110.76.

[5] M. Ogawa, S. Ishino, T. Mukai, D. Asano, N. Teramoto, H. Watabe, N. Kudomi, M. Shiomi, Y. Magata, H. Iida, et al., 18)F-FDG accumulation in atherosclerotic plaques: immunohistochemical and PET imaging study, J. Nucl. Med. 45 (2004) 1245–1250.

[6] A. Yamashita, Y. Zhao, S. Zhao, Y. Matsuura, C. Sugita, T. Iwakiri, N. Okuyama, K. Ohe, C. Koshimoto, K. Kawai, et al., Arterial (18)F-fluorodeoxyglucose uptake reflects balloon catheter-induced thrombus formation and tissue factor expression via nuclear factor-κB in rabbit atherosclerotic lesions, Circ. J. 77 (2013) 2626–2635, https://doi.org/10.1253/circj.cj-12-1463. Epub 2013 Jul 6.

[7] I.S. Rogers, K. Nasir, A.L. Figueroa, R.C. Cury, U. Hoffmann, D.A. Vermylen, T.J. Brady, A. Tawakol, Feasibility of FDG imaging of the coronary arteries: comparison between acute coronary syndrome and stable angina, JACC Cardiovasc Imaging 3 (2010) 388–397, https://doi.org/10.1016/j.jcmg.2010.01.004.

[8] I.S. Rogers, A. Tawakol, Imaging of coronary inflammation with FDG-PET: feasibility and clinical hurdles, Curr. Cardiol. Rep. 13 (2011) 138–144, https://doi.org/10.1007/s11886-011-0168-3.

[9] Y. Nitta, N. Tahara, A. Tahara, A. Honda, N. Kodama, M. Mizoguchi, H. Kaida, M. Ishibashi, N. Hayabuchi, H. Ikeda, S. Yamagishi, T. Imaizumi, Pioglitazone decreases coronary artery inflammation in impaired glucose tolerance and diabetes mellitus: evaluation by FDG-PET/CT imaging, JACC Cardiovasc Imaging 6 (2013) 1172–1182, https://doi.org/10.1016/j.jcmg.2013.09.004.

[10] A. Graham, Mitochondrial regulation of macrophage cholesterol homeostasis, Free Radic. Biol. Med. 89 (2015) 982–992, https://doi.org/10.1016/j.freeradbiomed.2015.08.010.

[11] N. Narayan, H. Mandhair, E. Smyth, S.G. Dakin, S. Kiriakidis, L. Wells, D. Owen, A. Sabokbar, P. Taylor, The macrophage marker translocator protein (TSPO) is down-regulated on pro-inflammatory 'M1' human macrophages, PLoS One 12 (2017), e0185767, https://doi.org/10.1371/journal.pone.0185767.

[12] J.L. Bird, D. Izquierdo-Garcia, J.R. Davies, J.H. Rudd, K.C. Probst, N. Figg, J.C. Clark, P.L. Weissberg, et al., Evaluation of translocator protein quantification as a tool for characterising macrophage burden in human carotid atherosclerosis, Atherosclerosis 210 (2010) 388–391, https://doi.org/10.1016/j.atherosclerosis.2009.11.047.

[13] O. Gaemperli, J. Shalhoub, D.R. Owen, F. Lamare, S. Johansson, N. Fouladi, A.H. Davies, O.E. Rimoldi, P.G. Camici, Imaging intraplaque inflammation in carotid atherosclerosis with 11C-PK11195 positron emission tomography/computed tomography, Eur. Heart J. 33 (2012) 1902–1910, https://doi.org/10.1093/eurheartj/ehr367.

[14] S. Hellberg, J.M.U. Silvola, M. Kiugel, H. Liljenbäck, N. Savisto, X.G. Li, A. Thiele, L. Lehmann, T. Heinrich, S. Vollmer, et al., 18-kDa translocator protein ligand 18F-FEMPA: biodistribution and uptake into atherosclerotic plaques in mice, J. Nucl. Cardiol. 24 (2017) 862–871, https://doi.org/10.1007/s12350-016-0527-y.

[15] S. Hellberg, H. Liljenbäck, O. Eskola, V. Morisson-Iveson, M. Morrison, W. Trigg, P. Saukko, S. Ylä-Herttuala, J. Knuuti, A. Saraste, et al., Positron Emission Tomography Imaging of Macrophages in Atherosclerosis with 18F-GE-180, a Radiotracer for Translocator Protein (TSPO), vol. 2018, Contrast Media Mol Imaging, 2018, p. 9186902, https://doi.org/10.1155/2018/9186902.

[16] C. Kopecky, E. Pandzic, A. Parmar, J. Szajer, V. Lee, A. Dupuy, A. Arthur, S. Fok, R. Whan, W.J. Ryder, et al., Translocator protein localises to CD11b+ macrophages in atherosclerosis, Atherosclerosis 284 (2019) 153–159, https://doi.org/10.1016/j.atherosclerosis.2019.03.011.

[17] A. Hatori, J. Yui, T. Yamasaki, L. Xie, K. Kumata, M. Fujinaga, Y. Yoshida, M. Ogawa, N. Nengaki, K. Kawamura, et al., PET imaging of lung inflammation with [18F]FEDAC, a radioligand for translocator protein (18 kDa), PLoS One 7 (2012), e45065, https://doi.org/10.1371/journal.pone.0045065.

[18] L. Xie, J. Yui, A. Hatori, T. Yamasaki, K. Kumata, H. Wakizaka, Y. Yoshida, M. Fujinaga, K. Kawamura, M.R. Zhang, Translocator protein (18 kDa), a potential molecular imaging biomarker for non-invasively distinguishing non-alcoholic fatty liver disease, J. Hepatol. 57 (2012) 1076–1082, https://doi.org/10.1016/j.jhep.2012.07.002.

[19] S.J. Chung, H. Youn, E.J. Jeong, C.R. Park, M.J. Kim, K.W. Kang, M.R. Zhang, G. J. Cheon, In vivo imaging of activated macrophages by 18F-FEDAC, a TSPO targeting PET ligand, in the use of biologic disease-modifying anti-rheumatic drugs (bDMARDs), Biochem. Biophys. Res. Commun. 506 (2018) 216–222, https://doi.org/10.1016/j.bbrc.2018.10.083.

[20] E. Falk, P.K. Shah, V. Fuster, Coronary plaque disruption, Circulation 92 (1995) 657–671, https://doi.org/10.1161/01.cir.92.3.657.

[21] R. Virmani, F.D. Kolodgie, A.P. Burke, A. Farb, S.M. Schwartz, Lessons from sudden coronary death: a comprehensive morphological classification scheme for atherosclerotic lesions, Arterioscler. Thromb. Vasc. Biol. 20 (5) (2000) 1262–1275.

[22] S. Cuhlmann, W. Gsell, K. Van der Heiden, J. Habib, J.L. Tremoleda, M. Khalil, F. Turkheimer, M.J. Meens, B.R. Kwak, J. Bird, et al., In vivo mapping of vascular inflammation using the translocator protein tracer 18F-FEDAA1106, Mol. Imag. 13 (2014), https://doi.org/10.2310/7290.2014.00014.

[23] D.Y. Hui, Intimal hyperplasia in murine models, Curr. Drug Targets 9 (3) (2008 Mar) 251–260, https://doi.org/10.2174/138945008783755601.

[24] I. Laitinen, P. Marjamäki, K. Någren, V.J. Laine, I. Wilson, P. Leppänen, S. Ylä-Herttuala, A. Roivainen, J. Knuuti, Uptake of inflammatory cell marker [11C] PK11195 into mouse atherosclerotic plaques, Eur. J. Nucl. Med. Mol. Imag. 36 (2009) 73–80, https://doi.org/10.1007/s00259-008-0919-6.

[25] K. Yanamoto, K. Kumata, T. Yamasaki, C. Odawara, K. Kawamura, J. Yui, A. Hatori, K. Suzuki, M.R. Zhang, [18F]FEAC and [18F]FEDAC: two novel positron emission tomography ligands for peripheral-type benzodiazepine receptor in the brain, Bioorg. Med. Chem. Lett 19 (2009) 1707–1710, https://doi.org/10.1016/j.bmcl.2009.01.093.

[26] K. Kim, D. Shim, J.S. Lee, K. Zaitsev, J.W. Williams, K.W. Kim, M.Y. Jang, H. Seok Jang, T.J. Yun, S.H. Lee, et al., Transcriptome analysis reveals nonfoamy rather than foamy plaque macrophages are proinflammatory in atherosclerotic murine models, Circ. Res. 123 (2018) 1127–1142, https://doi.org/10.1161/CIRCRESAHA.118.312804.

[27] M. Graebe, S.F. Pedersen, L. Højgaard, A. Kjaer, H. Sillesen, 18FDG PET and ultrasound echolucency in carotid artery plaques, JACC Cardiovasc Imaging 3 (2010) 289–295, https://doi.org/10.1016/j.jcmg.2010.01.001.